Thermal erosion patterns of permafrost peat plateaus in northern Norway

Léo C P Martin, Jan Nitzbon, Johanna Scheer, Kjetil S Aas, Trond Eiken, Moritz Langer, Simon Filhol, Bernd Etzelmüller, Sebastian Westermann

https://doi.org/10.5194/tc-2020-338
Preprint. Discussion started: 22 December 2020

The Cryosphere
Discussions
Open Access
EGU

Thermal erosion patterns of permafrost peat plateaus in northern Norway

Léo C.P. Martin[1,2*], Jan Nitzbon[3,4], Johanna Scheer[1,5], Kjetil S. Aas[1], Trond Eiken[1], Moritz Langer[3,4], Simon Filhol[1], Bernd Etzelmüller[1], Sebastian Westermann[1,6]

1. Department of Geosciences, University of Oslo, Blindern, 0316 Oslo, Norway
2. Faculty of Geosciences, Utrecht University, Utrecht, The Netherlands
3. Alfred Wegener Institute Helmholtz Centre for Polar and Marine Research, Telegrafenberg A45, 14473 Potsdam, Germany.
4. Geography Department, Humboldt-Universität zu Berlin, Unter den Linden 6, 10099 Berlin, Germany
5. Technical University of Denmark, Anker Engelunds Vej 1, Lyngby, Denmark
6. Center for Biogeochemistry in the Antropocene, Oslo, Norway

Correspondence to: Léo Martin (leo.doug.martin@gmail.com)

https://doi.org/10.5194/tc-2020-338
Preprint. Discussion started: 22 December 2020

The Cryosphere Discussions
Open Access
EGU

Abstract

Subarctic peatlands underlain by permafrost contain significant amounts of organic carbon and our ability to quantify the evolution of such permafrost landscapes in numerical models is critical to provide robust predictions of the environmental and climatic changes to come. Yet, the accuracy of large-scale predictions is so far hampered by small-scale physical processes that create a high spatial variability of surface ground thermal regime and thus of permafrost degradation patterns. In this regard, a better understanding of the small-scale interplay between microtopography and lateral fluxes of heat, water and snow can be achieved by field monitoring and process-based numerical modeling.

Here, we quantify the topographic changes of the Šuoššjávri peat plateau (Northern Norway) over a three-years period using repeated drone-based high-resolution photogrammetry. Our results show that edge degradation is the main process through which thermal erosion occurs and represents about 80 % of measured subsidence, while most of the inner plateau surface exhibits no detectable subsidence. Based on detailed investigation of eight zones of the plateau edge, we show that this edge degradation corresponds to a volumetric loss of 0.13 ± 0.07 m^3 yr^{-1} m^{-1} (cubic meter per year and per meter of plateau circumference).

Using the CryoGrid land surface model, we show that these degradation patterns can be reproduced in a modeling framework that implements lateral redistribution of snow, subsurface water and heat, as well as ground subsidence due to melting of excess ice. We reproduce prolonged climate-driven edge degradation that is consistent with field observations and present a sensitivity test of the plateau degradation on snow depth over the plateau. Small snow depth variations (from 0 to 30 cm) result in highly different degradation behavior, from stability to fast degradation.

These results represent a new step in the modeling of climate-driven landscape development and permafrost degradation in highly heterogeneous landscapes such as peat plateaus. Our approach provides a physically based quantification of permafrost thaw with a new level of realism, notably regarding feedback mechanisms between the dynamical topography and the lateral fluxes through which a small modification of the snow depth results in a major modification of the permafrost degradation intensity. In this regard, these results also highlight the major control of snow pack characteristics on the ground thermal regime and the benefit of improving snow representation in numerical models for permafrost degradation projections.

https://doi.org/10.5194/tc-2020-338
Preprint. Discussion started: 22 December 2020


The Cryosphere
Discussions
Open Access
EGU

28

29 1. Introduction

30 Observations show that permafrost is warming at a global scale (Biskaborn et al., 2019). Its
31 thawing has major consequences on Arctic and Boreal ecosystems and landscapes (Beck et al., 2015;
32 Farquharson et al., 2019; Liljedahl et al., 2016) and potentially represents an important climate feedback
33 through the degradation of thawed organic matter (Koven et al., 2015; Schuur et al., 2009, 2015). Carbon
34 emissions from permafrost regions towards the atmosphere are already observed (Natali et al., 2019);
35 field measurements show that these emissions are influenced by the timing of the active layer deepening
36 (Morgalev et al., 2017) and by the state of degradation of the permafrost terrains (Langer et al., 2015;
37 Nwaishi et al., 2020; Serikova et al., 2018). Particularly, abrupt thaw of ice-rich permafrost is expected
38 to become a dominant process regarding carbon emissions, offsetting the potential ecosystemic negative
39 feedback that is expected for gradual thaw (McGuire et al., 2018; Turetsky et al., 2020).

40 As such, our ability to quantify and represent the physical evolution of permafrost landscapes is
41 critical to provide robust predictions of the environmental and climatic changes to come (Aas et al.,
42 2019; Andresen et al., 2020; Teufel and Sushama, 2019). While permafrost affects about 14 millions
43 square kilometers throughout the Northern Hemisphere (Obu et al., 2019), the ground thermal response
44 to climatic signal and morphological changes of permafrost are governed by processes occurring within
45 a spatial scale of few meters (Gisnås et al., 2014; Jones et al., 2016; Martin et al., 2019; Way et al.,
46 2018). Indeed, at the small-scale, Arctic and Boreal permafrost landscapes in low lands (such as peat
47 plateaus and polygonal tundra) are characterized by low amplitude (0-3 m vertically) and high frequency
48 (10-100 m horizontally) spatial variations of their topography called microtopography (French, 2018).
49 On the one hand, microtopography drives the redistribution of snow, liquid water and heat and these
50 lateral fluxes can dramatically modify the ground thermal regime and water content (Martin et al., 2019).
51 On the other hand, permafrost microtopography result from the presence of excess ice in the ground (ice
52 content superior to natural porosity) and permafrost thawing drives surface subsidence ("thermokarst",
53 Göckede et al., 2017, 2019; Nitzbon et al., 2019, 2020). However, the representation of this feedback
54 between small-scale fluxes and dynamical topography in numerical models is still in its infancy. Robust

https://doi.org/10.5194/tc-2020-338
Preprint. Discussion started: 22 December 2020

predictions of the physical state of permafrost landscapes thus require further field observations and numerical developments to refine our understanding of these phenomena.

Peat plateaus are permafrost landforms covering extensive regions throughout the Boreal and Arctic realms which store nearly 200 Pg of carbon (Lindgren et al., 2018). They are mainly located in the sporadic permafrost zone (Seppälä, 1972; Sollid & Sørbel, 1998) and are typically associated with a climatic envelope characterized by a mean annual ground temperature around 0°C and limited precipitation (< 800 mm yr^{-1}) (Aalto et al., 2017; Parviainen and Luoto, 2007). Permafrost underneath peat plateaus is thus relatively warm and its distribution is highly sensitive to climate changes (Aalto et al., 2014, 2017; Fronzek et al., 2010; Luoto et al., 2004). The limit of continuous and discontinuous permafrost in the North Hemisphere is already moving northward (Thibault and Payette, 2009) and peat plateaus 'degradation is observed in the North American Arctic (Jones et al., 2016; Mamet et al., 2017; Payette et al., 2004), Fennoscandia (Borge et al., 2017) and Western Siberia (Jones et al., 2016; Sherstyukov and Sherstyukov, 2015). In Northern Norway, the analysis of aerial imagery showed a decrease between 33 and 71 % in the lateral extent of the peat plateaus since the 1950's (Borge et al., 2017), with the largest lateral changes since the 2000's. These results suggest that "lateral erosion" (as coined by Borge et al., 2017) plays a crucial role in permafrost degradation.

The ongoing degradation of Fennoscandian peat plateaus is a potential analogue for the future of much larger peat plateau areas found in Russia, Canada and Alaska. It provides the opportunity for field measurements and process-based approaches to further understand the local drivers of permafrost peatland thermal dynamics. Several studies contributed to understand how microtopography drives the lateral fluxes of heat, water and snow and to quantify their influence on the ground thermal regime with both field measurements and numerical modeling experiments (Martin et al., 2019; Sannel, 2020; Sannel et al., 2016; Sjöberg et al., 2016). The snow and water transport from the plateau towards the surrounding mire is critical to maintain important surface temperature difference between them (1.5 to 2°C of mean annual temperature at 1m depth, Martin et al. 2019). It affects the subsurface thermal regime and enables the presence of permafrost in regions where the mean annual air temperature is above 0°C (Jones et al., 2016; Martin et al., 2019; Sannel and Kuhry, 2011). However, a comprehensive model that could

https://doi.org/10.5194/tc-2020-338
Preprint. Discussion started: 22 December 2020

simulate the landscape evolution (including observed thermal erosion patterns) in a quantitative process-based fashion is lacking.

Here, we quantify volume changes of a peat plateau in Northern Norway using repeated digital elevation models compiled from drone aerial imagery. The surface topography of the plateau was reconstructed and compared for the years 2015 and 2018 using drone-based photogrammetry. Subsequently, we adapt the laterally coupled tiled version of the CryoGrid model (Langer et al., 2016; Nitzbon et al., 2019; Westermann et al., 2016) to reproduce observed patterns of microtopography change, including an analysis of model sensitivity towards snow depth. The work presented here prolongates the field observations and numerical simulations of Martin et al. (2019). Besides, it also builds on recent studies dedicated to numerical modelling of the ground thermal regime, lateral heat, snow and water fluxes and dynamical topography in arctic landscapes (Aas et al., 2019; Nitzbon et al., 2019, 2020).

2. Study area: the Šuoššjávri peat plateaus

The Šuoššjávri site (69.38° N, 24.25° E, around 310 m asl, Fig. 2) is situated in Finnmarksvidda, Northern Norway, and extends over approximately 23 ha. A detailed presentation of the Šuoššjávri peat plateaus can be found in Martin et al. (2019), and a map detailing the geomorphological context around the study site is presented in the Supplementary Material (Fig. A2). The climate of Finnmarksvidda (Fig. 1) is continental with mean annual air temperature ranging from -4°C to -2°C (Aune, 1993) and mean annual precipitation of less than 400 mm. The Šuoššjávri site consists of a laterally carved peat plateaus and smaller peat mounds surrounded by wet mires and ponds. These peat bodies extend over meters to several tens of meters with tortuous horizontal geometries and rise 0.1 m to 3 m above the surrounding wet mire (Fig. 2). Several of the peat plateau edges show signs of advanced degradation and lateral erosion. The stratigraphy of the plateau and its spatial variability are presented in Sect. 3.3.3. Literature results for this site are discussed in Sect. 4.

https://doi.org/10.5194/tc-2020-338
Preprint. Discussion started: 22 December 2020

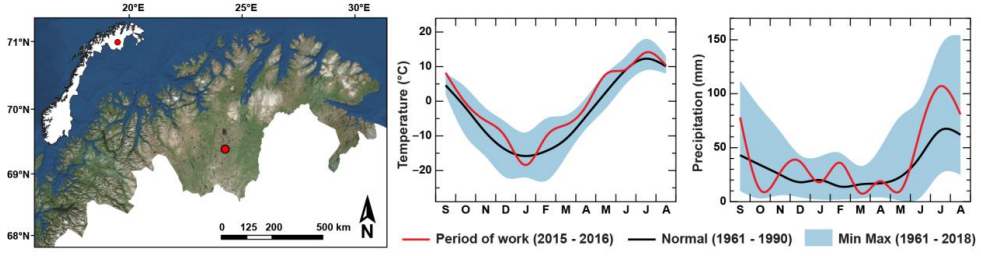

Figure 1. Location and climate of the study site (Šuoššjávri, Finnmark). The red curve on the temperature and precipitation graphs correspond to the study period (2015-2016). The black curves indicate normal values and the bleu shading the minimum and maximum values over the 1961–2018 period. Data from the Cuovddatmohkki station (no. 97350) located at 286 m asl, 7 km east from Šuoššjávri (310 m asl). Data from the Norwegian Meteorological Institute (sharki.oslo.dnmi.no). Landsat satellite image (ESRI). All three panels of the figure are from Martin et al. (2019).

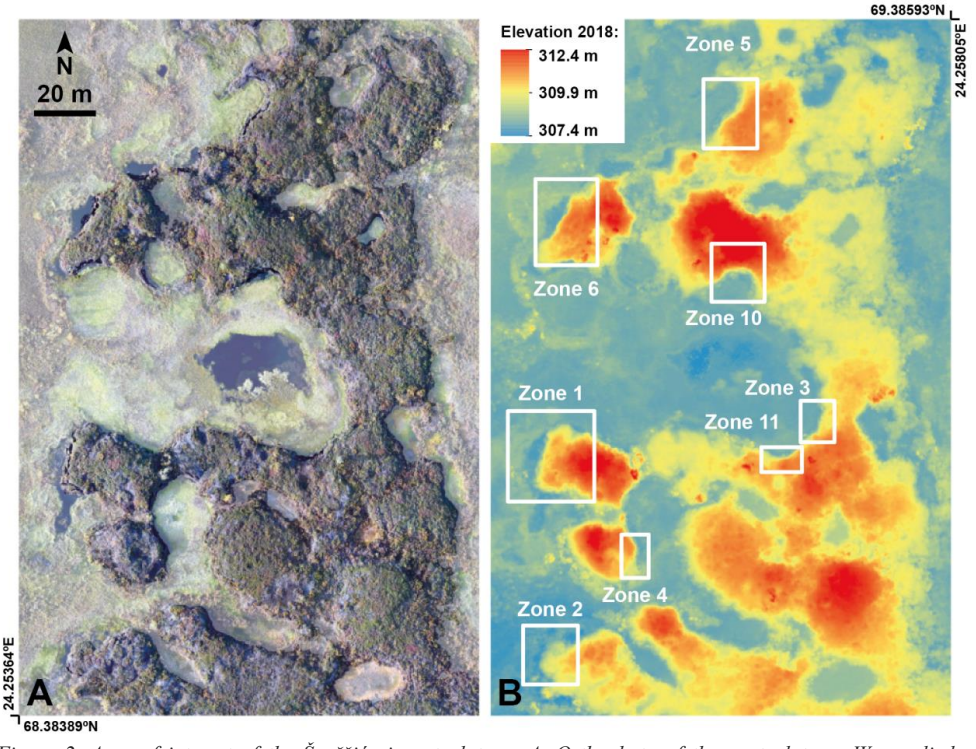

Figure 2. Area of interest of the Šuoššjávri peat plateau. A. Orthophoto of the peat plateau. We applied a transparent white shading on the mire to better distinguish it from the plateau. B. Digital Elevation Model of the plateau in 2018. The edge transect areas on which this study focuses are indicated with white boxes.

https://doi.org/10.5194/tc-2020-338
Preprint. Discussion started: 22 December 2020

3. Material and methods

3.1. Field measurements

We used drone-based structure from motion photogrammetry to compute a high-resolution digital elevation model (DEM) of the Šuoššjávri peat plateau. Aerial imagery was acquired thanks to a digital camera mounted on a drone during two flights in September 2015 and 2018 (02/09/2015 and 05/09/2018). Flights were done 120 m above the ground and the photo acquisition presented a side overlap of 40 % and a forward overlap of 80 %. The horizontal and vertical coordinates of natural and artificial ground control points were acquired with a differential GPS (dGPS) to support the topographic reconstruction. Images were processed, including the ground control points, using the Agisoft Photoscan software (version 1.2.6). The final digital elevation models have a grid resolution of 0.1 m. To guarantee a meaningful subsidence signal, we only considered subsidence values exceeding 5 cm in this study.

To frame our modeling approach with field constraints, we measured snow depth on the Šuoššjávri peat plateau. Snow measurements for winter 2016 were presented in Martin et al. (2019). Here we extend these measurements to winters 2017 and 2018 for the plateau top part only. Snow depth was measured in the end of March with an avalanche probe at precise locations covering the top of the plateau, as defined in Martin et al. (2019). The exact location of each measurement point under the snow was localized using a dGPS system to ensure a 5–10 cm horizontal accuracy.

3.2. Quantification of thermal erosion patterns

Our drone-based photogrammetric approach (Sect. 3.1) enabled us to derive repeat DEMs of the peat plateau for September 2015 and 2018. We computed the elevation difference (elevation from 2018 minus elevation from 2015) to quantify the spatial pattern of elevation changes of the plateau. From this elevation difference map, we selected eight degrading zones (later referred as *edge transect areas*) presenting a 10-30 m long and roughly straight lateral extent for comparison with modeling results (Sect. 3.3). Based on the changes of elevation and lateral extent of the plateau between 2015 and 2018, we used the eight edge transect areas (Fig. 2) to calculate the subsided volume per meters of circumference and per year ($m^3\ m^{-1}\ yr^{-1}$). Because elevation changes occurred in the mire due to water level variations

https://doi.org/10.5194/tc-2020-338
Preprint. Discussion started: 22 December 2020

between the two dates, we relied on an estimation of the elevation of the plateau edge inflection point (around 309.7-309.8 m asl, yellow color on Fig. 2B) to delimitate the plateau from the mire and thus identify elevation changes associated to the plateau only.

Permafrost degradation creates different subsidence patterns depending on the size of the permafrost landform. Small structures like palsas tend to sink entirely from the edge to the top, while peat plateaus show stability of their top part and pronounced lateral retreat. To distinguish between these two types of thermal erosion patterns, we introduce a so-called *Horizontal vs Vertical* (HvsV) shape index that we can apply to both field observations and model results. The basic concept of the HvsV index is illustrated in Fig. 3. To compute the HvsV index, the plateau edge elevation is averaged over five points, from its very base (z_1) to the first meters where its flat top is reached (z_5). The elevation difference between 2015 and 2018 (Δz) for z_1, z_2, z_4 and z_5 is then used as follow:

$$HvsV\ shape\ index = \max\left(0,\ 1 - \frac{\Delta z_4 + \Delta z_5}{\Delta z_1 + \Delta z_2}\right) \qquad (1)$$

For the field observations, the HvsV index was obtained by first laterally averaging the slope of each edge transect area using five to fourteen parallel elevation profiles across the zone, for the 2015 and 2018 DEMs. These two synthetic elevation profiles were then averaged into the five required points (from the edge to the top of the plateau). The HvsV index was then calculated based on these synthetic elevation differences (between 2018 and 2015).

For the simulation results (Sect. 4.2), a 10 m long window was used to capture the topography from the base of the plateau to its flat top. These 10 m profiles where then averaged into the five required points. Then, elevation differences were observed over three-year-long time periods to compute the HvsV index.

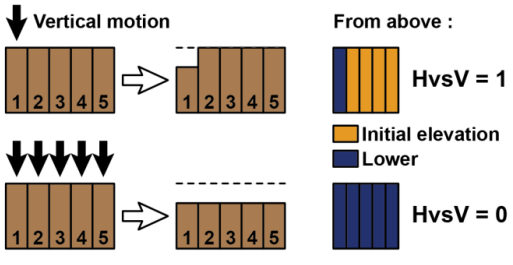

Figure 3. Presentation of the HvsV index used to quantify the observed and simulated degradation types. The index evolves from 1 when the plateau undergo pure lateral degradation (subsidence restricted to the areas at contact with the mire) and 0 when it experiences a global collapse (subsidence of all the areas).

https://doi.org/10.5194/tc-2020-338
Preprint. Discussion started: 22 December 2020

3.3. Modeling climate-induced changes of peat plateau topography

3.3.1 The CryoGrid3 model

We simulate the ground thermal regime and related topographic evolution of the Šuoššjávri peat plateau using the CryoGrid model (Westermann et al., 2016). CryoGrid is a land surface model designed for permafrost modeling. It consists of a physically based description of 1D heat transfer in the soil column, including freeze–thaw process of soil water/ice. The model features a simple snowpack module, which includes heat conduction, dynamic buildup, melt, sublimation, water infiltration, and refreezing. CryoGrid uses a surface energy balance module to calculate the ground surface temperature. The turbulent fluxes of sensible and latent heat are calculated using a Monin – Obukhov approach (Monin and Obukhov, 1954). Evapotranspiration is adjusted to soil moisture and the water uptake is distributed vertically so that it decreases exponentially with depth. The soil moisture computation along the soil column relies on a bucket scheme (Martin et al., 2019, Nitzbon et al., 2019).

CryoGrid represents ground subsidence resulting from the melt of the excess ice in the ground (thermokarst process, see Westermann et al., 2016). Subsidence calculation is based on soil stratigraphy (ice content and natural porosity) and modifies the 1D vertical soil mesh when excess ice (soil grids for which the ice content exceeds the natural soil porosity) melts. This functionality was first implemented in Westermann et al. (2016) and later used in (Nitzbon et al., 2019, 2020) to represent the transient evolution of polygonal tundra landscapes caused by permafrost degradation for various hydrological scenarios. In the present study, this scheme is used to account for the thermal erosion of the peat plateaus and the microtopography changes induced by permafrost degradation within the plateau.

Following Nitzbon et al. (2019, 2020), CryoGrid includes a parallel framework to simultaneously compute several 1D tiles that can exchange numerical information at defined time steps (quantities of water, snow and heat). This approach, denoted as *laterally coupled tiling*, allows us to couple 1D tiles with different stratigraphies/topographies. With this method, the spatial variability tied to Arctic landscape such as the topographic gradient between the center and the rim of polygonal tundra (Nitzbon et al., 2019) or the stratigraphy differences between Yedoma and Holocene deposits (Nitzbon et al., 2020) has been simulated. It also permits to calculate the lateral fluxes of snow, subsurface water

https://doi.org/10.5194/tc-2020-338
Preprint. Discussion started: 22 December 2020

and heat that are small-scale key drivers of the ground thermal regime (Nitzbon et al., 2019). In the present study, laterally coupled tiling is used to simulate the Šuoššjávri peat plateau and its interface with the surrounding wet mire and represent the subsidence and lateral fluxes along this transition (Sect. 3.2.4).

3.3.2 Modelling framework and sensitivity analysis to plateau snow depth

Snow depth is a major parameter influencing the ground thermal regime (cf. Introduction) and assessing its influence on the degradation dynamics of peat plateau is one of the objectives of this study. Because of microtopography-dependent wind-driven snow redistribution, snow depths over the peat plateaus are usually shallow (10-40 cm, Martin et al. 2019). In the Cryogrid model, the efficiency of this redistribution is adjusted with a parameter that sets, for each tile, the maximum snow depth which cannot be transported towards the mire. Snow accumulated beyond this depth is systematically transported by the model towards the lower-lying tiles, here representing the mire.

The present-day topography of the peat plateau is clear evidence that the long-term evolution is not only governed by thermal erosion of the plateau edges, but also by a complex interplay of thermokarst process in the interior of the plateau, with pond formation and drainage, as well as drainage gully development and deepening. As a full three-dimensional simulation of these phenomena is beyond the capability of present-day models, we focus modeling on the simplified situation of a laterally symmetric peat plateau edge. Furthermore, we conduct simulations for steady-state climate forcing from the period of the field observations (Sect. 3.3.3). This makes it possible to compare the magnitudes of modeled volumetric plateau degradation over three-year periods with field observations for sufficiently straight sections of the plateau edge (Sect. 3.2, Fig. 2). As field observations of snow depth reveal a considerable spread of snow depths values on the plateau (that cannot be reproduced by modeling), we investigate the sensitivity of modeled topography changes towards snow depths on the plateau (which can be controlled by the above mentioned model parameter), using a realistic range of values between which snow depths vary during the simulations (Sect. 3.1). We therefore designed four simulations called: *0 cm snow*, *5-10 cm snow*, *10-20 cm snow* and *20-30 cm snow*.

https://doi.org/10.5194/tc-2020-338
Preprint. Discussion started: 22 December 2020

221 ### *3.3.3 Model setup*

222 To simulate the edge thermal erosion of the Šuoššjávri peat plateau, we used the laterally
223 coupled tiling framework of CryoGrid (Nitzbon et al., 2019) with 40 coupled tiles in a linear
224 configuration so that they can exchange snow, subsurface water and heat (Sect. 3.2.1). In the third
225 dimension, translational symmetry is assumed in order to represent the evolution of the 10 to 30 meters
226 long and roughly straight geometry of these specific zones of the plateau. These edge transect areas are
227 detailed in Fig. 2.

228 Fig. 4 provides details on the model setup. The wet mire is divided into three tiles with surface
229 elevation at 300 m asl. They are composed of a 3 m thick layer of unfrozen saturated peat above a 7 m
230 thick silty mineral layer that also extends below the plateau. Their respective widths are 50, 2 and 0.5
231 m. These values are significantly higher than those of the tiles initially hosting permafrost to ensure
232 stable unfrozen lateral boundary conditions in the mire side, as is observed in the plateau mire complex.
233 The largest and most external mire tile is linked to a hydrologic reservoir (Nitzbon et al., 2019) to ensure
234 a steady water level in the mire at its surface (at 300 m asl), keeping it always saturated and preventing
235 ponding of surface water above 300 m asl. The peat plateau tiles are 0.3 m wide, giving a total width of
236 the plateau of 11.1 m. It stands at 302 m asl, making it 2 m high, in line with observations (Table 1). For
237 the initial steady state simulation (Sect. 3.2.5), the topographic transition between the mire and the
238 plateau was initially set as an arbitrary regular slope between 300 and 302 m asl as well as the active
239 layer depths, which were linearly interpolated between 0.9 m (at the contact with the mire) and 0.7 m at
240 the other hand of the plateau. The excess ice is distributed homogeneously along depth and the soil grid
241 ice content is set so that the plateau surface reaches 300 m asl (mire surface elevation) when the excess
242 ice is fully melted.

https://doi.org/10.5194/tc-2020-338
Preprint. Discussion started: 22 December 2020

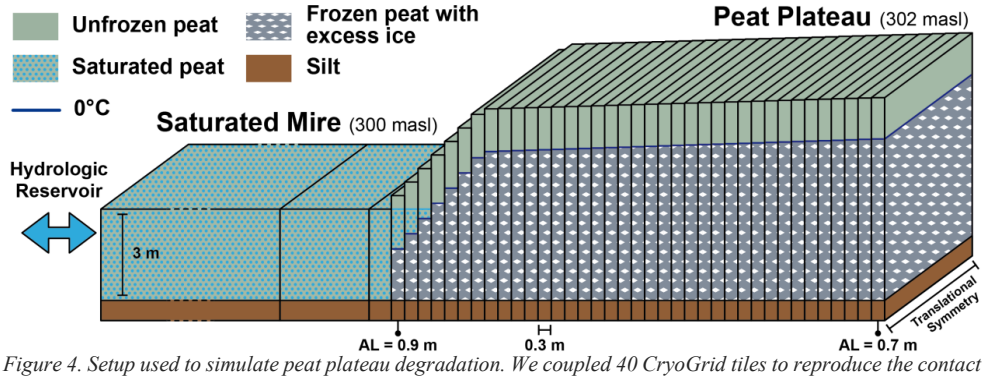

Figure 4. Setup used to simulate peat plateau degradation. We coupled 40 CryoGrid tiles to reproduce the contact between the mire and the peat plateau. The AL occurrences indicate the active layer used for the CryoGrid tiles with permafrost. We linearly interpolated them between 0.9 and 0.7 m. The model implement lateral fluxes of snow, subsurface water and heat between the tiles as well as ground subsidence due to excess ice melt.

3.3.4 Steady state climatic forcing and model spin-up

As presented in Martin et al. (2019), we obtained the forcing data for the model with a dynamical downscaling of the ERA Interim reanalysis data (Dee et al., 2011). We used for this Weather Research and Forecasting model (WRF v.3.8.1; Skamarock and Klemp, 2008) with an option set as in Aas et al. (2016) with the exceptions mentioned in Martin et al. (2019). We used the nearest grid points in the 3-km domain to derive the forcing data for CryoGrid. In Finnmark, the hydrological year 2015–2016 revealed itself to be particularly warm. Both 2015 and 2016 ranged 2 to 3°C above the 1961 - 1990 normal period. Additionally, the period was wetter than average, with 2015 and 2016 being, respectively, 33 and 50 % wetter than the normal period. As such, the simulated period gives a good opportunity to study the response of ground surface temperature to an anomalously warm and wet 12 month-long climatic conditions (Grinde et al., 2018; Heiberg et al., 2017). This is of particular interest for this study because both of these two factors enhance permafrost degradation (Sect. 1).

The forcing data are looped to generate 100-year time series with steady-state climate forcing. To achieve a realistic initial temperature profile also in deeper layers, a 100-year spin-up is performed for all simulations using the 0 cm snow scenario, for which the peat plateau is stable (Sect. 4.2). Note that the other snow scenarios cannot be used for model spin-up, as the plateau edge starts to retreat instantly, so that a true steady-state cannot be reached.

https://doi.org/10.5194/tc-2020-338
Preprint. Discussion started: 22 December 2020

265 *3.3.5 Input parameters*

266 Similar to Martin et al. (2019), the soil stratigraphy used in the model is based on analyzed soil
267 samples from the peat plateau site of Iškoras located 40 km east from Šuoššjávri, the site of the present
268 study. Consistently with Kjellman et al. (2018), the results we obtained consist of a 3 meters thick peat
269 soil layer with 5 % of mineral and 15 % of organic material in total volumetric content (and thus a 80 %
270 porosity), underlain by a 7 m saturated mineral silt layer with 50 % porosity, above a mineral bedrock
271 layer (3 % porosity, as in Westermann et al., 2013).

272 Over the Šuoššjávri plateau, the soil stratigraphy presents a significant spatial variability. While
273 the above described stratigraphy matches the western parts of the plateau, on the eastern and southern
274 parts, organic soil thickness is limited by the near surface underlying morainic deposits. Doing manual
275 soil probing, we encountered mineral soil within the first meter in the close vicinity of the plateau. Such
276 stratigraphy is not prone to subsidence and for this reason the modeling work presented here focuses on
277 reproducing the subsidence patterns observed on the western part of the peat plateau where edge already
278 started retreating (Borges et al., 2017).

279 Snow and soil parameters are based on the field measurements and the sensitivity tests from
280 Martin et al. (2019). The simulations use a snow density of 230 kg m^{-3}, consistent with measurements
281 on top of the peat plateaus. Similarly, the soil field capacity used for the simulations is set to 0.55 (in
282 terms of volumetric water content). Peat soil field capacity can display a pronounced variability (20 to
283 60 % of the volumetric content; Walczak and Rovdan, 2002) and our value is consistent with field
284 observation from Southern Siberian peatlands (Motorin et al., 2017). All other parameters (e.g. the
285 surface energy balance parameterization etc.) were chosen as in Martin et al. (2019).

https://doi.org/10.5194/tc-2020-338
Preprint. Discussion started: 22 December 2020


The Cryosphere Discussions
Open Access
EGU

4. Results

4.1 Measurements of microtopography evolution

The topographic changes of the Šuoššjávri peat plateau between September 2015 and September 2018 are presented in Fig. 5. From the DEM difference, we found that 19 % of the plateau exhibits 5 cm or more subsidence (i.e. the sensitivity threshold of the measurements), which consequently implies that 81 % of the plateau is stable during the observation period. The mean subsidence value (considering values larger than 5 cm) is 17±15 cm (1σ) and the median 12 cm, with 1.2 % the total plateau surface subsiding by more than 40 cm. The maximum observed subsidence is a one square meter patch in Zone 6, exhibiting between 1.5 and 1.7 m of subsidence over the 3 years.

We extracted the plateau edge over its outermost 2 m (i.e. the band of the 20 outermost pixels delimiting the plateau). We find that this surface corresponds to one third of the total plateau surface, but represents 77 % of the total subsidence (including the rims of the depressions within the plateau). The distribution of subsidence values for the whole plateau and its edge only are presented in Fig. 6.

Due to the differences in peat plateau stratigraphies detailed in Sect. 3.3.3., the west side of the plateau features higher subsidence values than the east side. On the eastern edge, ground subsidence is lower due to the limited thickness of the peat layer, with mineral soil at a depth of less than one meter below the surface. A description of the eight edge transect areas and their subsidence between 2015 and 2018 is presented in Table 1. For these eight zones, the average volumetric loss per year (normalized by the structure length, i.e. the length of the plateau edge of the different sections) is 0.13±0.08 m^3 m^{-1} yr^{-1}. The mean HvsV shape index (Sect. 3.2.) is 0.78±0.08, which suggests a dominance of horizontally- over vertically-driven ground subsidence.

https://doi.org/10.5194/tc-2020-338
Preprint. Discussion started: 22 December 2020

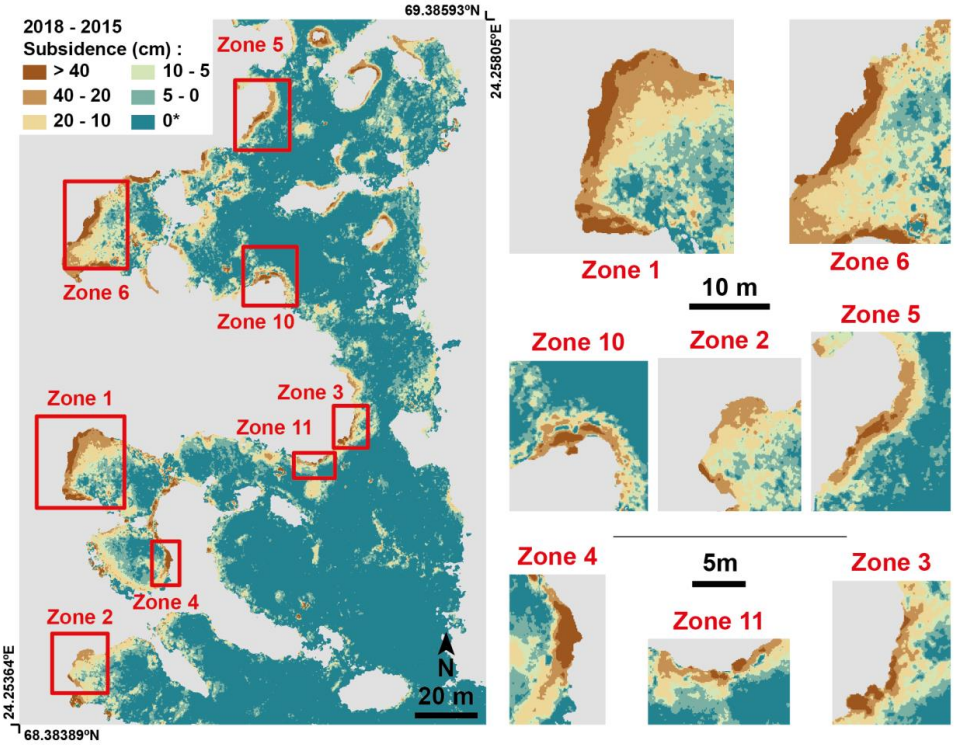

Figure 5. Subsidence over the Šuoššjávri peat plateau. Left: Overview of the subsidence on the plateau. Note that the color scale is truncated for subsidence values higher than 40 cm and lower than 0 cm, which ,for the latter, correspond to increase in surface elevation due to vegetation change. Right: Edge transect areas of the plateau used to compare observed and simulated degradation patterns (Sect. 3.2.1).

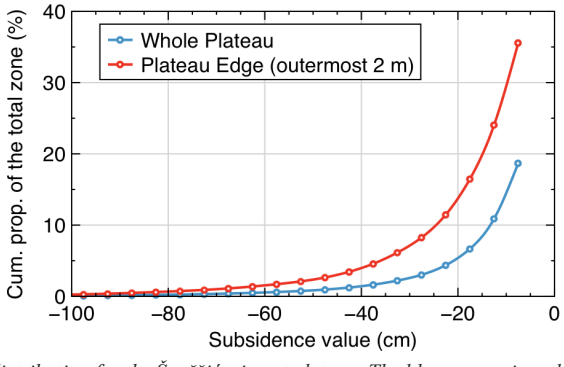

Figure 6. Subsidence distribution for the Šuoššjávri peat plateau. The blue curve gives the subsidence distribution for the whole plateau while the red one gives it for the plateau edge only. The edge is taken as the outermost 2 m of the plateau. Only subsidence values greater than 0.05 m are considered in this graph to guarantee a meaningful subsidence signal. Data are derived from the topography difference between 2015 and 2018. Percentages indicate which proportion of the total area (whole plateau or plateau edge) is affected by a subsidence superior (in absolute value) or equal to a given subsidence value (e.g. 36 % of the edge exhibits a subsidence higher than or equal to 5 cm).

https://doi.org/10.5194/tc-2020-338
Preprint. Discussion started: 22 December 2020

Zone	Palsa Height (cm)	Structure Length (m)	Subsided volume per structure length ($m^3/m/a$)	HvsV Shape Index (-)
1	200	25	0.295	0.74
2	130	16	0.100	0.64
3	120	16	0.074	0.68
4	140	13	0.132	0.81
5	120	25	0.045	0.94
6	180	30	0.232	0.75
10	220	13	0.124	0.81
11	145	11	0.052	0.84
		Mean	**0.132**	**0.78**
		Standard Dev.	**0.078**	**0.08**

Table 1. Field observations at the 8 edge transect areas presented in Fig. 2. Elevation changes and surface measurements are derived from the digital elevation models. The HvsV shape index (Fig. 3) was calculated according to equation (1). See Sect. 3 for more details.

Snow measurement results are presented in Fig. 7. Consistently with Martin et al. (2019), peat plateau tops are commonly covered with 10 to 40 cm of snow, with most of the values between 10 and 30 cm. We used these observations to design the numerical simulations presented in this study and their four different snow depths: 0, 5-10, 10-20 and 20-30 cm (Sect. 3.3.2).

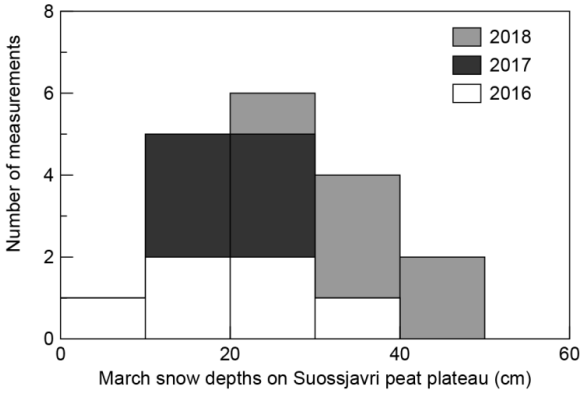

Figure 7. March snow depth distribution on top of the Šuoššjávri peat plateau for 2016, 2017 and 2018. Data for 2016 are from Martin et al. (2019).

4.2 Simulations of microtopography evolution

Results from the model simulations are presented in Fig. 8. The temporal evolution of the peat plateau microtopography shows an edge retreat, while a large part of the plateau is stable, as observed on the field. The temporal evolution and patterns of edge retreat exhibit a pronounced dependence on

https://doi.org/10.5194/tc-2020-338
Preprint. Discussion started: 22 December 2020

the snow depth on the peat plateau. The *0 cm snow* simulation (with complete transport of the snow from the plateau towards the mire) shows no thermal erosion of the plateau, whereas the simulation with the thinnest snow depth (*5-10 cm snow*) triggers an edge retreat of 4 to 5 meters over the 100 years duration of the simulation. For the *10-20 cm snow* and *20-30 cm snow* simulations, the plateau fully degrades within the simulation time with notable differences in profile evolution between simulations. While the plateau fully degrades at the end of the 100 years simulation for the *10-20 cm snow* simulation, it occurs within 40 years for the *20-30 cm snow* simulation.

The topographic evolution observed over the three simulations lead us to identify three different types of simulated thermal erosion. For both the *5-10 cm snow* and *10-20 cm snow* simulations, the plateau degradation first shows a phase of slope adjustment during which the slope profile smooths from year to year. We denote this phase as the "Initial Slope Adjustment" (ISA, Fig. 8 and 9). This phase lasts for 40 years in the *5-10 cm snow* simulation and 30 years for the *10-20 cm snow* simulation. For the same two simulations, the thermal erosion later affects the slope in a more uniform way and the plateau edge retreats with a constant slope at a constant rate; during 60 years for the *5-10 cm snow* simulation and 20 years for the *10-20 cm snow* one. We denote this phase the "Constant Edge Degradation" (CED, Fig. 8 and 9). During the second half of the *10-20 cm snow* simulation, both the edge and the top of the plateau subside. We denote this phase as the "Plateau Collapse" (PC, Fig. 8 and 9). Contrary to the *10-20 cm snow* simulation, the *20-30 cm snow* simulation does not exhibit the phases of initial slope adjustment and constant edge degradation but only the evolution corresponding to a plateau collapse.

https://doi.org/10.5194/tc-2020-338
Preprint. Discussion started: 22 December 2020

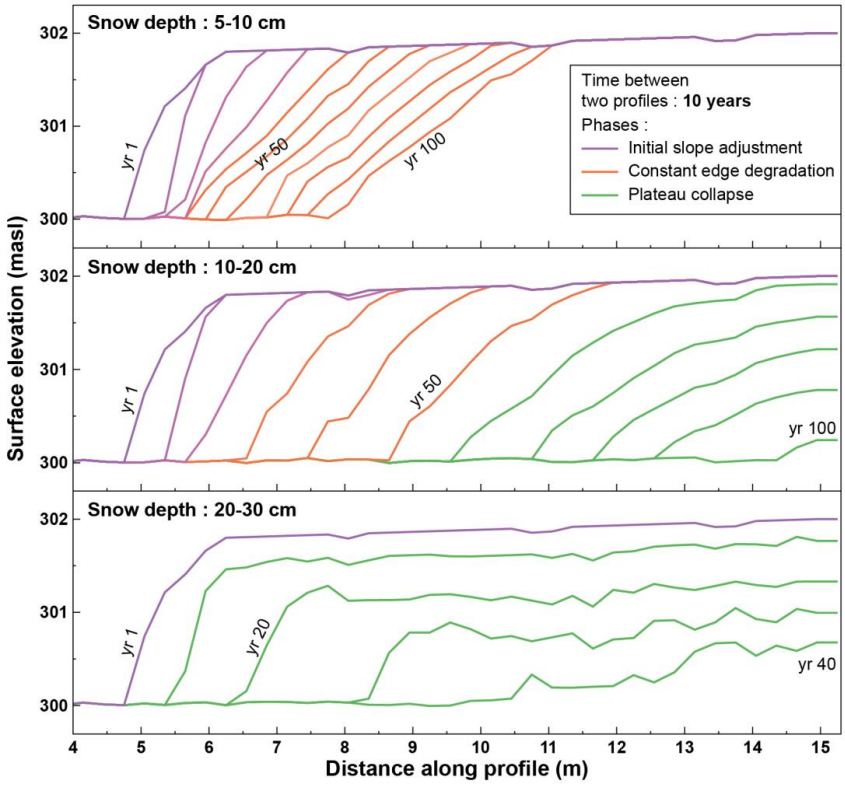

Figure 8. Surface elevation profiles of the peat plateaus as simulated with CryoGrid for different snow depths on top of the plateau, in time increments of 10 years. The evolution between the lines lead us to identify different periods in the plateau degradation: Initial Slope Adjustment (slope modifications along time), Constant Edge Degradation (slope conserved) and Plateau Collapse (subsidence over the full plateau). Note that the "0 cm snow" simulation did not produce any subsidence and for this reason, does not appear on this figure.

The top panel of Fig. 9 presents the volumetric rate loss of the plateau for the three simulations. For the *5-10 cm snow* simulation, this rate is constant around 0.06 to 0.08 m^3 lost per meter of lateral extension of the plateau (i.e. per meter of plateau circumference) and per year (m^3 m^{-1} yr^{-1}) for the whole simulation. For the *10-20 cm snow* simulation, the volumetric loss during the initial slope adjustment and the constant edge degradation phases shows a steady increase from 0.08 to 0.28 m^3 m^{-1} yr^{-1}. During the plateau collapse phase, this rate steadily decreases to 0.12 m^3 m^{-1} yr^{-1} at the end of the simulation. For the *20-30 cm snow* simulation, the rate reaches 0.28 m^3 m^{-1} yr^{-1} over the first decades and stabilizes at this value for 10-20 years before undergoing another rapid increase to 0.35 m^3 m^{-1} yr^{-1}, at which it stabilizes until the end of the simulation. Further quantification of the thermal erosion is given in Sect. 4.3. A comparison between simulated and measured ground surface temperatures (temperature logger

https://doi.org/10.5194/tc-2020-338
Preprint. Discussion started: 22 December 2020

time series from Martin et al., 2019) is presented in the supplementary material (Fig. A1), showing an overall good agreement.

4.3 Comparison of model results and topographic measurements

A comparison of the Šuoššjávri peat plateau thermal erosion patterns between the field data and the simulations is presented in the two bottom panels of Fig. 9. Field values are displayed in grey and represent average and standard deviation of the field measurements of the respective measured variables (Sect. 3.3 and Table 1). For each simulation, we average the volume loss and shape index over the degradation periods presented in Sect. 4.2 (ISA,CED,PC).

Field-based and simulated values are in good agreement regarding volume changes. The mean field value (0.13±0.08 m^3 m^{-1} yr^{-1}) is compatible with the different degradation phases observed for the *5-10 cm snow* and *10-20 cm snow* simulations. The *5-10 cm snow* simulation shows little spread and smaller values than the average field value (< 0.1 m^3 m^{-1} yr^{-1} in absolute value) whereas the *10-20 cm snow* simulation shows greater spread and greater volume changes than the average field value (between 0.1 and 0.25 m^3 m^{-1} yr^{-1}). The *20-30 cm snow* simulation stands out from this trend and exhibits volume losses substantially higher than the field values (> 0.25 m^3 m^{-1} yr^{-1}).

Regarding the HvsV shape index, the Initial Slope Adjustment phases for both the *5-10 cm snow* and the *10-20 cm snow* simulations exhibit values of 1, slightly larger than the field value (0.84±0.09). Both Constant Edge Degradation phases are in line with field observations, exhibiting a greater spread among the simulations than among the field values. Because both are characterized by simultaneous edge degradation and global subsidence, the two plateau collapse phases (for the *10-20 cm snow* and *20-30 cm snow* simulations) have HvsV values significantly smaller than the field values (<0.6).

https://doi.org/10.5194/tc-2020-338
Preprint. Discussion started: 22 December 2020

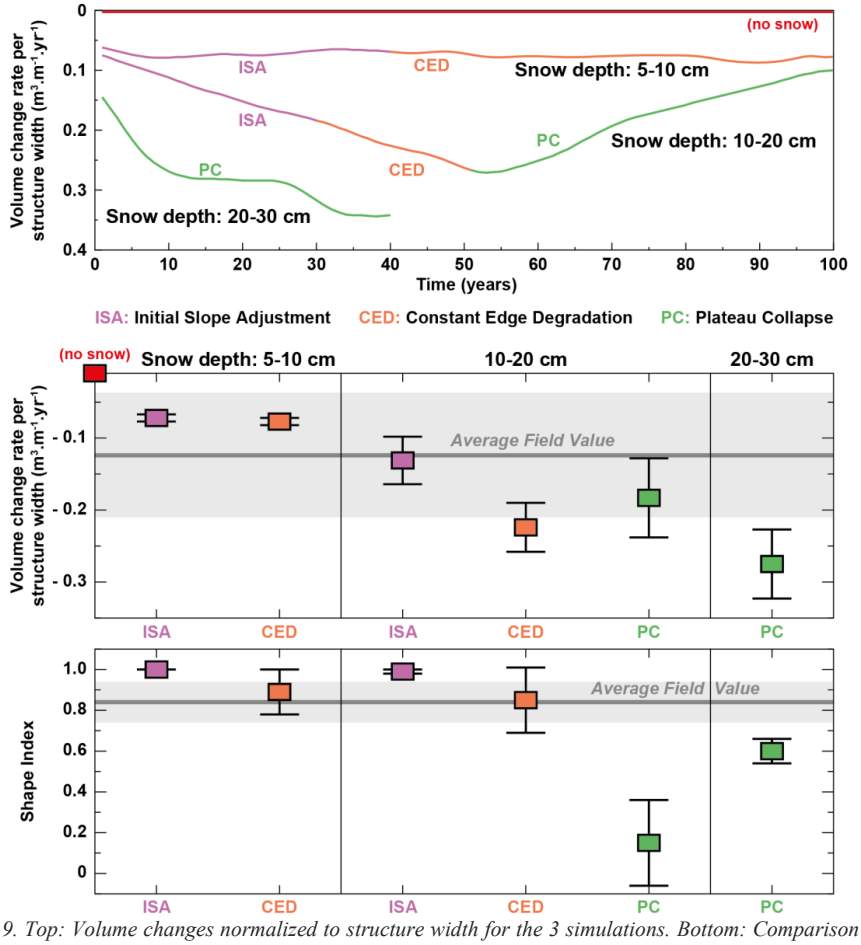

Figure 9. Top: Volume changes normalized to structure width for the 3 simulations. Bottom: Comparison of the degradation patterns between observations and simulations. Observations are means and standard deviations of the variables measured in the eight edge transect areas presented in Table 1. They appear as a grey line and shading. The values derived from simulations are mean and standard deviations taken over the different periods of the simulations. As detailed in Fig. 8, the profile evolution allows identifying different periods in the plateau evolution, namely Initial Slope Adjustment (ISA), Constant Edge Degradation (CED) and Plateau Collapse (PC). The red square reminds that no subsidence was observed for the "0 cm snow" simulation.

https://doi.org/10.5194/tc-2020-338
Preprint. Discussion started: 22 December 2020


The Cryosphere Discussions
Open Access
EGU

5. Discussion

5.1 Field measurements

At the western edge of the Šuoššjávri plateau, subsidence is highly variable, ranging from 0 to more than 1 meter within 3 years. This pattern highlights the chaotic behavior of permafrost landscapes facing degradation due to a positive feedback between subsidence, snow accumulation and water drainage. When an initial perturbation, such as intense rainfall or extraordinary snow accumulation triggers subsidence (Seppälä, 1988, 2011), both the snow redistribution and the subsurface drainage towards the mire are affected, which creates warmer surface conditions and, in return, triggers more subsidence. Considering the complex geometry of the Šuoššjávri plateau edges, meter-scale variability of the snow and hydrological conditions likely contribute to observed variability of ground subsidence. Besides, due to the dependence of heat transfer to the surface area of the interface between the mire and the plateau, the geometry of edges affects degradation speed. As such, zones 1, 2, 4 and 6 belong to convex features of the plateau edges and show particularly high subsidence rates.

Our results confirm that edge degradation is a major degradation pathway of peat plateaus with 77 % of the total subsidence occurring within the outermost 2 meters of the Šuoššjávri plateau. This result shows consistency with Jones et al. (2016) who reported that 85 % of the degradation of forested permafrost plateaus was due to lateral degradation along the margins. Estimating the elevation of the inflection point of the plateau edge from the DEMs allows to quantify the plateau surface area at a given time, even though in practice the precise positioning of such limit can be discussed. Between 2015 and 2018, we find that the Šuoššjávri plateau lost 3.2 % of its surface area. If we take the percentage of annual loss rate of plateau area as $100 * (1 - S_{i+1}/S_i)$ (where the fraction corresponds to the ratio between the area at year i and the area at year i+1), then over an observation period of n years, the average ratio can be expressed as:

$$r = 100 \times \left(1 - \sqrt[n]{\frac{S_n}{S_0}}\right) \quad (2)$$

Where r is the annual loss rate in % yr^{-1}, n is the number of year between the 2 observations, S_n the plateau surface at the end of the observation period and S_0 the plateau surface at the beginning of the

https://doi.org/10.5194/tc-2020-338
Preprint. Discussion started: 22 December 2020

424 period. Applying Eq. 2, the aerial change in this study corresponds to a surface loss rate of 1.1 % yr^{-1}.
425 Reconstructing the Šuoššjávri peat plateau extent from 1956 to 2011 with aerial imagery, Borge et al.
426 (2017) observed annual loss rates that they compared to the 1956 extension. Using Eq. 2, we compute
427 the annual loss rate from their data to be 0.5 % yr^{-1} from 1956 to 1982, 0.8 % yr^{-1} from 1982 to 2003
428 and of 1.4 % yr^{-1} from 2003 to 2011. Hence, our retreat rate is in good agreement with the long-term
429 edge retreat rates, although the two values cannot be compared in a strict sense, since Borge et al. (2017)
430 also included small palsas in the surrounding area (which show faster degradation rates than the peat
431 plateau) in their assessments.

432 5.2 Model results

433 *5.2.1 The plateau degradation*

434 Our modeling framework relies on an idealized geometry and steady-state climate forcing, so the
435 full variety of the observed degradation patterns cannot be reproduced. However, the comparison
436 between model results and observations clearly shows that the numerical model framework can capture
437 the correct order of magnitude of the degradation processes, while also reproducing key patterns in the
438 observed ground temperature regime (supplementary material, Fig. A1).
439 Among the different degradation phases (Initial Slope Adjustment, Constant Edge Degradation and
440 Plateau Collapse), the ISA and PC phases are less relevant than the CED phase for model to field
441 comparisons: the ISA phase is strongly affected by the initial response of the model to the applied
442 climate forcing and snow depths on the plateau, whereas the CED phase corresponds to the prolonged
443 edge retreat observed in the field, while the bulk of the peat plateau remains stable. The PC phase
444 corresponds to the sustained collapse of the plateau with ground subsidence in all parts, which is not
445 observed for the Šuoššjávri peat plateau, but regularly occurs for smaller circular palsas in the vicinity.
446 For such palsas, the assumption of translational symmetry inherent in the model setup is not valid and
447 simulations should be performed assuming rotational rather than translational symmetry. This suggests
448 that our simulations are indeed most realistic during the CED phase, whereas changes of the peat plateau
449 shape need to be taken into account to model the final stages of degradation.

https://doi.org/10.5194/tc-2020-338
Preprint. Discussion started: 22 December 2020

450 *5.2.2 The role of snow*

451 Our simulations confirm the crucial role of snow on the ground thermal regime and peat plateau
452 degradation. The sensitivity of modeled ground temperatures towards snow depth is in good agreement
453 with the field measurements for the Šuoššjávri and the Iškoras peat plateau (40 km east of Šuoššjávri)
454 presented by Martin et al. (2019). For example, they showed that the measurement points on the plateau
455 exhibiting a mid-march snow depth smaller than 10 cm were associated with coldest mean annual
456 ground temperatures, and that 70 % of the plateau locations with stable permafrost had a March snow
457 depth smaller than 30 cm.

458 However, our idealized model approach assumes snow depths to be constant on the peat plateau,
459 which does not capture the significant spatial and interannual variability of snow depths on the plateau
460 observed in measurements (Fig. 7). In particular, the complex geometry of snow drift patterns (snow
461 accumulation) along the plateau edges, with snow drifts forming on lee sides, is not captured by the
462 simple snow redistribution model implemented in CryoGrid. Field observations show that snow drifts
463 along the plateau edges feature considerably higher snow depths than the surrounding wet mire, thus
464 introducing additional winter warming in the zone of maximum change. Additionally, persistent wind
465 patterns can strongly influence the distribution of snowdrifts. Unfortunately we do not possess field
466 measurements to discuss this parameter at the Šuoššjávri site. In CryoGrid, on the other hand, snow
467 removed from the plateau is evenly distributed over the entire mire, not taking edge effects into account.

468 Furthermore, our model assumes a fixed value for the snow density and thus snow thermal
469 properties, while this parameter in reality varies with e.g. snow depth and time, responding strongly to
470 synoptic conditions and imposing metamorphosis of the snowpack. Measurements of snow density in
471 Šuoššjávri showed that the snow on top of palsas is slightly less dense than in the mire. This could be
472 due to a thinner snowpack leading both to greater kinematic metamorphism and the formation of depth
473 hoar, notorious for high porosity and a real difficulty to measure density and high effective thermal
474 conductivity (Domine et al., 2016). A thinner snowpack also implies a lower overburden load and
475 therefore less compaction. Such limitations could be moderated by using more sophisticated snow
476 models taking snow microphysics and the transient evolution of snow density into account, such as
477 CROCUS (Vionnet et al., 2012) or SNOWPACK (Bartelt and Lehning, 2002). Yet, even these models

https://doi.org/10.5194/tc-2020-338
Preprint. Discussion started: 22 December 2020

show limitations to reproduce the thermal characteristics of snow deposited in Arctic regions because they do not account for the vapor fluxes in the snow pack, which significantly affect the snow thermal conductivity profile (Domine et al., 2016).

5.3 Implications for climate driven permafrost landscapes changes

5.3.1 Sensitivity to climate forcing and perturbations

In this study, we present idealized numerical simulations of peat plateau thermal erosion that reproduce the general patterns of edge retreat as observed in-situ through repeat digital elevation models. We demonstrate that the snow depth on the plateau is a strong control for subsidence patterns and dynamics. This result indicates that peat plateau systems will react sensitively to changes in the applied climate forcing, not only regarding temperature but also regarding (snow) precipitation and windspeed variations which all affects in turn snow pack building. In this regard, predictions regarding snow fall for the coming decades are complex. An overall decrease of mean snowfall is expected at the global scale (O'Gorman, 2014), consistently with observed trends over the past decades (Liston and Hiemstra, 2011) but this decrease will be accompanied by strong regional trend (Brown and Mote, 2009; Lader et al., 2020) and the frequency and distribution of extreme snowfall remain unclear (O'Gorman, 2014). In any case, it appears that for future modelling works, the accuracy of both the snowpack buildup and its thermal properties at the small-scale (10-100 m) should be considered of major importance to robustly simulate permafrost degradation.

Additionally, our implementation illustrates the idea of small-scale feedback mechanism on permafrost degradation. The feedback between the dynamical microtopography and the lateral fluxes shows how a limited increase in snow cover (when comparing the *10-20 cm snow* and the *20-30 cm snow* simulations) results in a dramatically faster degradation rate. Such a sensitivity to minor perturbation resulting into major modifications of permafrost degradation finds consistency with the observed permafrost destabilization when punctually augmenting the snow depth with a fence (Hinkel and Hurd, 2006), when implanting linear road infrastructures (Deimling et al., 2020) or due to the traffic of heavy vehicle in Alaskan lowlands (Raynolds et al., 2020).

https://doi.org/10.5194/tc-2020-338
Preprint. Discussion started: 22 December 2020

5.3.2 *Spatiotemporal stability and degradation conditions*

Our simple approach is clearly not able to capture the complex patterns of different subsidence rates that are observed around the edges of the plateau (Fig. 5). On top of small-scale variations of ground stratigraphy, excess ice contents and plateau heights, we suggest that the irregular plateau outline with both concave and convex shapes also affects the lateral fluxes of heat, water and snow, which in turn exert a control on the edge dynamics. While computationally demanding, our multi-tile approach could be embedded in an ensemble framework to represent a range of edge geometries and other critical parameters, yielding a range of different degradation scenarios and therefore capture the high spatial variability of subsidence at the plateau scale.

Over longer time scales, future studies should clarify if the simple multi-tile setup can capture climate-induced changes of peat plateau stability, for example between the cold Little Ice Age (when most of the present-day peat plateaus were formed, Kjellman et al., 2018) and the warmer conditions of the 20th century during which peat plateaus in Finnmark likely entered their current state of accelerating degradation (e.g. Borge et al., 2017).

5.3.3 *Permafrost modeling with Land Surface Models*

Most Land Surface Models (LSMs) used to simulate the future response of permafrost to climate changes still rely on simplified one-dimensional implementations of permafrost thaw dynamics which ignores subsidence and only reflects gradual top-down thawing of the frozen ground (Andresen et al., 2020). Excess ice melt and the resulting microtopography changes exert a major control on the evolution of hydrologic conditions, which in turn greatly influence the timing of permafrost degradation, as demonstrated for polygonal tundra (Nitzbon et al., 2019, 2020). Aas et al., (2019) presented a similar approach for peat plateaus in Northern Norway. It is based on two tiles (one for the wet mire, one for the plateau) and reproduces both climate-induced stability and degradation. However, in this approach, the plateau subsides as a whole when a climate-related threshold is exceeded and excess ice begins to melt. This contrasts with our field observations, which show ongoing edge retreat on decadal timescales, while the plateau interior is largely stable. Our approach uses a larger number of tiles to explicitly represent the temperature and soil moisture gradients across the plateau edges, which causes excess ice

https://doi.org/10.5194/tc-2020-338
Preprint. Discussion started: 22 December 2020

melt to only occur in a narrow zone at the plateau edge, in agreement with our observations. Over longer timescales, on the other hand, this process leads to the reshaping and finally the complete collapse of the entire peat plateau. In ESMs, implementing a multi-tile approach is challenging due to its complexity and computational demands. Yet, parameterized approaches could likely be developed, based on sensitivity tests using our framework. In particular, future studies should investigate to what extent the two-tile approach demonstrated by Aas et al. (2019) can emulate the results of the multi-tile model, especially when averaging the results over the range of climatic conditions under which peat plateaus occur in the sub-Arctic domain. However, a multi-tile setup would probably reveal different hydrological regimes (zones of well-drained plateaus would remain until the end), which would in turn affect carbon decomposition.

6. Conclusion

We present and compare field measurements and numerical modeling of thermal erosion patterns of the Šuoššjávri peat plateau in Northern Norway. We use high resolution digital elevation models derived from drone-based photogrammetry to quantify changes of surface elevations of the plateau between September 2015 and 2018. Thermal erosion of the plateau edges is the main process through which thermal erosion occurs and accounts for 80 % of the total measured subsidence (in terms of subsided soil volume), while most of the total plateau surface exhibits no detectable subsidence. We show that this retreat corresponds to a volumetric loss of 0.13 ± 0.07 m^3 m^{-1} yr^{-1} for the edge transect zones we studied.

Using the CryoGrid land surface model we show that these degradation patterns can be reproduced numerically in a framework that implements lateral redistribution of snow, subsurface water and heat, as well as excess-ice-melt-triggered subsidence. Overall, the modeled volumetric change rates are in the same order of magnitude as the measurements. Based on a steady-state climate forcing, our simulations demonstrate the importance of lateral snow transport and resulting snow depths on the plateau. The modelled peat plateau is fully stable when all snow on its top is transported towards the mire (0 cm snow depth on the plateau), whereas its edges degrade at increasing rates with increasing snow depths. While

https://doi.org/10.5194/tc-2020-338
Preprint. Discussion started: 22 December 2020

a maximum of 5-10 cm on the plateau only triggers a 4-5 meters edge retreat within 100 years, a 10-20 cm cover fully degrades the plateau in 100 years and a 20-30 cm cover degrades it in 40 years. Our simulations reproduce the observed lateral edge degradation with a stable plateau top, but the final phase of plateau degradation corresponds to complete plateau collapse with subsidence occurring throughout the entire plateau.

These results highlight the fast and high spatial variability of permafrost landscape evolution in response to climate change. They also show that the related microtopographic, thermal and hydrological modifications can be represented in numerical models, opening the way for substantial improvements in simulating permafrost landscape evolution and its impact on greenhouse gas emissions from thawing permafrost.

Author contribution. L.M. and S.W. designed the study and conducted the numerical simulations. L.M. led the manuscript preparations. S.W., M.L., J.N. and L.M. contributed to the model development. T.E., S.W., L.M., J.S. acquired field data. K.A. provided forcing data. L.M. and S.F. analyzed field data. All authors contributed to result interpretation and to manuscript preparation.

Code availability. The model code and settings used for the simulations is available from github.com/CryoGrid/CryoGrid3/tree/xice_mpi_palsa_newsnow. It will be permanently deposited upon acceptance of the manuscript. The code is published under the GNU General Public License v3.0.

Data availability. Field data will be permanently deposited on archive.sigma2.no upon acceptance of the manuscript.

Competing interests. The authors declare that they have no conflict of interest.

Acknowledgements. This work was funded by PERMANOR (Norwegian Research Council, KLIMAFORSK program, NFR project 255331), Nunataryuk (EU grant agreement no. 773421) and the Department of Geosciences of the University of Oslo, Norway. WRF simulations were performed on the Abel high- performance computing facility with resources provided by the Department of Geosciences of Oslo University. The land surface simulations were performed on resources provided by UNINETT Sigma2 - the National Infrastructure for High Performance Computing and Data Storage in Norway The authors declare that they have no conflicts of interests. All data are available in the manuscript or the Supplementary Material.

https://doi.org/10.5194/tc-2020-338
Preprint. Discussion started: 22 December 2020

The Cryosphere Discussions
Open Access
EGU

Appendix A: Model output comparison with field measurements

Fig. A1 compares the Mean Annual Ground Surface Temperatures (MAGST) and the Active Layer Thickness (ALT) as they are simulated in this study and in Martin et al. (2019) with field measurements from the same study. Overall, both simulation works yield similar results and show good agreement with field measurements.

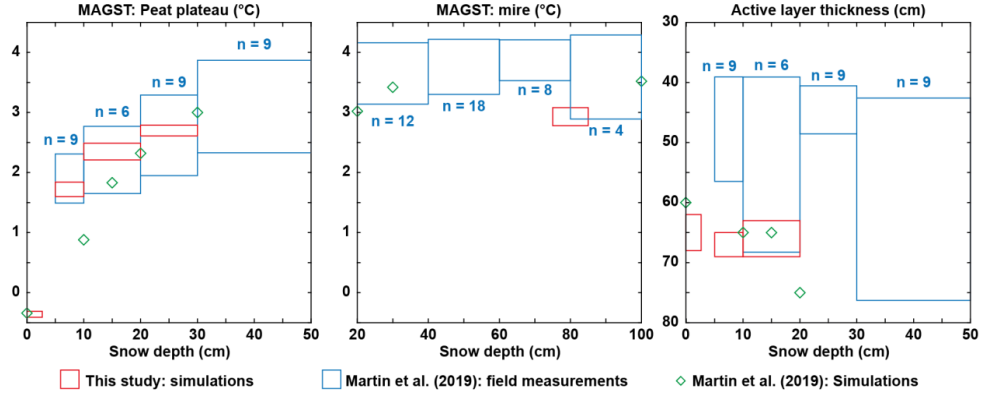

Figure A1. Mean Annual Ground Temperature (MAGST) and Active layer thickness as they are simulated in this study and in Martin et al. (2019) compared to the field measurements from Martin et al. (2019) for the same region. Values indicated with the letter n correspond to the number of field observations in Martin et al. (2019).

While MAGSTs from the present study are in perfect agreement with the measured ones on the peat plateau, the model seems to underestimates them slightly (0.5°C too cold) in the mire. This in mainly due to a too low water inflow from the reservoir which does not manage to always fully saturate the wet mire. As a consequence, the uppermost layer of the mire partially dries during summer, which shifts the heat flux during autumn from latent to sensible and imposes colder temperatures in the mire during winter.

Active layers are overestimated by 20 to 30 cm for snow depths smaller than 10 cm. This probably arises from the difference between the real and simulated snow conditions. While real conditions can be erratic and show important variations during winter (from snow free to snow covered, back and forth), snow scenarios in the simulations are smoother and show a prolonged covered conditions, leading to deeper ALT.

https://doi.org/10.5194/tc-2020-338
Preprint. Discussion started: 22 December 2020

The Cryosphere
Discussions
Open Access
EGU

Appendix B: Geomorphological settings

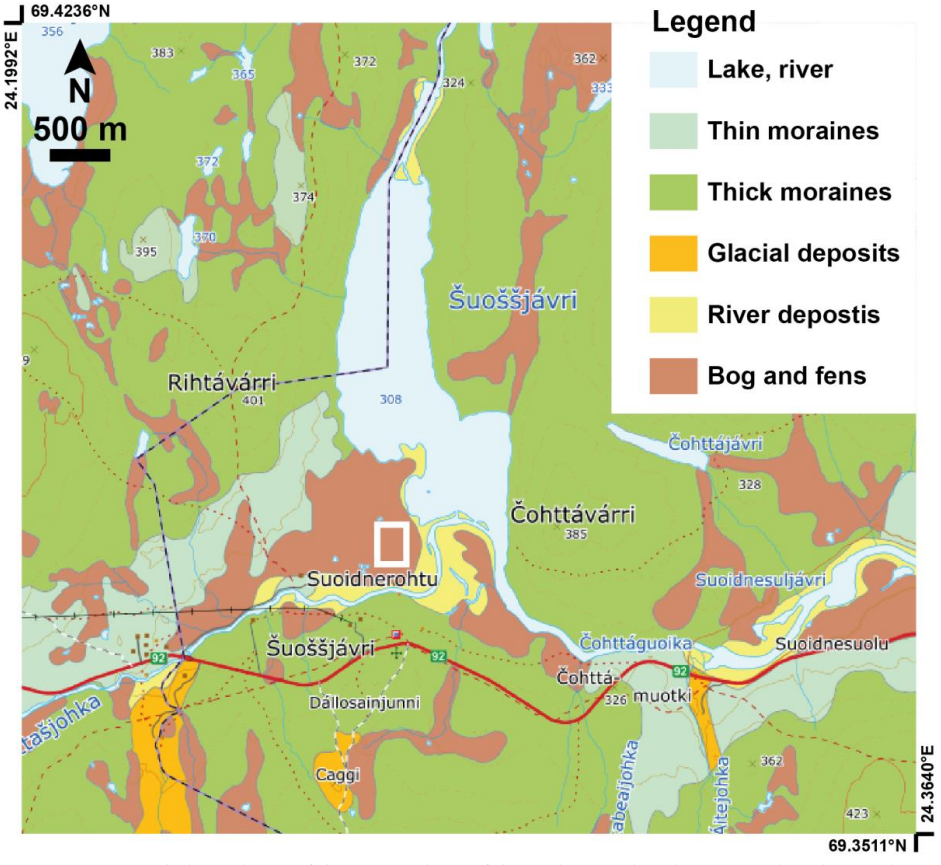

Figure A2. Geomorphological map of the surroundings of the study site. The white rectangle indicates the study site. Source: Geological Survey of Norway (NGU).

References

Aalto, J., Venäläinen, A., Heikkinen, R. K. and Luoto, M.: Potential for extreme loss in high-latitude Earth surface processes due to climate change, Geophys. Res. Lett., 41(11), 3914–3924, doi:10.1002/2014GL060095, 2014.

Aalto, J., Harrison, S. and Luoto, M.: Statistical modelling predicts almost complete loss of major periglacial processes in Northern Europe by, Nat. Commun., 8(1), 1–8, doi:10.1038/s41467-017-00669-3, 2017.

Aas, K. S., Dunse, T., Collier, E., Schuler, T. V., Berntsen, T. K., Kohler, J. and Luks, B.: The climatic mass balance of Svalbard glaciers: a 10-year simulation with a coupled atmosphere–glacier mass balance model, Cryosph., 10(3), 1089–1104, doi:10.5194/tc-10-1089-2016, 2016.

Aas, K. S. K. S., Martin, L., Nitzbon, J., Langer, M., Boike, J., Lee, H., Berntsen, T. K. T. K. and Westermann, S.: Thaw processes in ice-rich permafrost landscapes represented with laterally coupled tiles in a land surface model, Cryosph., 13(2), 591–609, doi:10.5194/tc-13-591-2019, 2019.

Andresen, C. G., Lawrence, D. M., Wilson, C. J., McGuire, A. D., Koven, C., Schaefer, K., Jafarov, E., Peng, S., Chen, X., Gouttevin, I., Burke, E., Chadburn, S., Ji, D., Chen, G., Hayes, D. and Zhang, W.: Soil moisture and

https://doi.org/10.5194/tc-2020-338
Preprint. Discussion started: 22 December 2020

hydrology projections of the permafrost region – a model intercomparison, Cryosph., 14(2), 445–459, doi:10.5194/tc-14-445-2020, 2020.

Aune, B.: Temperaturnormaler, normalperiode 1961-1990, Nor. Meteorol. Inst. Rapp. Klima, 1993, 1–63, 1993.

Bartelt, P. and Lehning, M.: A physical SNOWPACK model for the Swiss avalanche warning, Cold Reg. Sci. Technol., 35(3), 123–145, doi:10.1016/S0165-232X(02)00074-5, 2002.

Beck, I., Ludwig, R., Bernier, M., Strozzi, T. and Boike, J.: Vertical movements of frost mounds in subarctic permafrost regions analyzed using geodetic survey and satellite interferometry, Earth Surf. Dyn., 3(3), 409–421, doi:10.5194/esurf-3-409-2015, 2015.

Biskaborn, B. K., Smith, S. L., Noetzli, J., Matthes, H., Vieira, G., Streletskiy, D. A., Schoeneich, P., Romanovsky, V. E., Lewkowicz, A. G., Abramov, A., Allard, M., Boike, J., Cable, W. L., Christiansen, H. H., Delaloye, R., Diekmann, B., Drozdov, D., Etzelmüller, B., Grosse, G., Guglielmin, M., Ingeman-Nielsen, T., Isaksen, K., Ishikawa, M., Johansson, M., Johannsson, H., Joo, A., Kaverin, D., Kholodov, A., Konstantinov, P., Kröger, T., Lambiel, C., Lanckman, J.-P., Luo, D., Malkova, G., Meiklejohn, I., Moskalenko, N., Oliva, M., Phillips, M., Ramos, M., Sannel, A. B. K., Sergeev, D., Seybold, C., Skryabin, P., Vasiliev, A., Wu, Q., Yoshikawa, K., Zheleznyak, M. and Lantuit, H.: Permafrost is warming at a global scale, Nat. Commun., 10(1), 264, doi:10.1038/s41467-018-08240-4, 2019.

Borge, A. F., Westermann, S., Solheim, I. and Etzelmüller, B.: Strong degradation of palsas and peat plateaus in northern Norway during the last 60 years, Cryosph., 11(1), 1–16, doi:10.5194/tc-11-1-2017, 2017.

Brown, R. D. and Mote, P. W.: The Response of Northern Hemisphere Snow Cover to a Changing Climate*, J. Clim., 22(8), 2124–2145, doi:10.1175/2008JCLI2665.1, 2009.

Deimling, T. S. Von, Lee, H., Ingeman-nielsen, T., Westermann, S., Romanovsky, V., Lamoureux, S., Walker, D. A., Chadburn, S., Cai, L., Nitzbon, J., Jacobi, S. and Langer, M.: Consequences of permafrost degradation for Arctic infrastructure - bridging the model gap between regional and engineering scales, , (September), 1–31, 2020.

Domine, F., Barrere, M. and Sarrazin, D.: Seasonal evolution of the effective thermal conductivity of the snow and the soil in high Arctic herb tundra at Bylot Island , Canada, , 2573–2588, doi:10.5194/tc-10-2573-2016, 2016.

Farquharson, L. M., Romanovsky, V. E., Cable, W. L., Walker, D. A., Kokelj, S. V. and Nicolsky, D.: Climate Change Drives Widespread and Rapid Thermokarst Development in Very Cold Permafrost in the Canadian High Arctic, Geophys. Res. Lett., 46(12), 6681–6689, doi:10.1029/2019GL082187, 2019.

French, H. M.: The periglacial environment, Fourth Edition, John Wiley & Sons Ltd., Chichester, England. [online] Available from: https://www.wiley.com/en-us/The+Periglacial+Environment%2C+4th+Edition-p-9781119132783, 2018.

Fronzek, S., Carter, T. R., Räisänen, J., Ruokolainen, L. and Luoto, M.: Applying probabilistic projections of climate change with impact models: a case study for sub-arctic palsa mires in Fennoscandia, Clim. Change, 99(3–4), 515–534, doi:10.1007/s10584-009-9679-y, 2010.

Gisnås, K., Westermann, S., Schuler, T. V., Litherland, T., Isaksen, K., Boike, J. and Etzelmüller, B.: A statistical approach to represent small-scale variability of permafrost temperatures due to snow cover, Cryosphere, 8(6), 2063–2074, doi:10.5194/tc-8-2063-2014, 2014.

Göckede, M., Kittler, F., Kwon, M. J., Burjack, I., Heimann, M., Kolle, O., Zimov, N. and Zimov, S.: Shifted energy fluxes, increased Bowen ratios, and reduced thaw depths linked with drainage-induced changes in permafrost ecosystem structure, Cryosph., 11(6), 2975–2996, doi:10.5194/tc-11-2975-2017, 2017.

Göckede, M., Kwon, M. J., Kittler, F., Heimann, M., Zimov, N. and Zimov, S.: Negative feedback processes following drainage slow down permafrost degradation, Glob. Chang. Biol., 25(10), 3254–3266, doi:10.1111/gcb.14744, 2019.

Grinde, L., Heiberg, H., Kristiansen, S., Mamen, J., Gangstø Skaland, R., Szewczyk-bartnicka, H. and Tilley Tajet, H. T.: Været i Norge, Klimatologisk oversikt, Året 2017, Oslo. [online] Available from: https://www.met.no/publikasjoner/met-info/met-info-2017/_/attachment/download/06c46052-3343-4e67-9cb2-fa43ad4f0f46:1d260f20cc2299d9a2d196a3c5f6fe63e44abfaf/MET-info-13-2017.pdf, 2018.

Heiberg, H., Kristiansen, S., Mamen, J., Gangstø Skaland, R., Szewczyk-Bartnicka, H. and Tilley Tajet, H. T.: Været i Norge, Klimatologisk oversikt, Året 2016, Oslo. [online] Available from: https://www.met.no/publikasjoner/met-info/met-info-2016/_/attachment/download/c8e579ab-da7a-4e10-84c8-

https://doi.org/10.5194/tc-2020-338
Preprint. Discussion started: 22 December 2020

c7ed108ef47f:3a738a02dcc931e0e46a743a8bdc5fcab6fa8ed0/MET-info-13-2016.pdf, 2017.

Hinkel, K. M. and Hurd, J. K.: Permafrost destabilization and thermokarst following snow fence installation, Barrow, Alaska, U.S.A., Arctic, Antarct. Alp. Res., 38(4), 530–539, doi:10.1657/1523-0430(2006)38[530:PDATFS]2.0.CO;2, 2006.

Jones, B. M., Baughman, C. A., Romanovsky, V. E., Parsekian, A. D., Babcock, E. L., Stephani, E., Jones, M. C., Grosse, G. and Berg, E. E.: Presence of rapidly degrading permafrost plateaus in south-central Alaska, Cryosph., 10(6), 2673–2692, doi:10.5194/tc-10-2673-2016, 2016.

Koven, C. D., Schuur, E. A. G., Schädel, C., Bohn, T. J., Burke, E. J., Chen, G., Chen, X., Ciais, P., Grosse, G., Harden, J. W., Hayes, D. J., Hugelius, G., Jafarov, E. E., Krinner, G., Kuhry, P., Lawrence, D. M., MacDougall, A. H., Marchenko, S. S., McGuire, A. D., Natali, S. M., Nicolsky, D. J., Olefeldt, D., Peng, S., Romanovsky, V. E., Schaefer, K. M., Strauss, J., Treat, C. C. and Turetsky, M.: A simplified, data-constrained approach to estimate the permafrost carbon–climate feedback, Philos. Trans. R. Soc. A Math. Phys. Eng. Sci., 373(2054), 20140423, doi:10.1098/rsta.2014.0423, 2015.

Lader, R., Walsh, J. E., Bhatt, U. S. and Bieniek, P. A.: Anticipated changes to the snow season in Alaska: Elevation dependency, timing and extremes, Int. J. Climatol., 40(1), 169–187, doi:10.1002/joc.6201, 2020.

Langer, M., Westermann, S., Walter Anthony, K., Wischnewski, K. and Boike, J.: Frozen ponds: production and storage of methane during the Arctic winter in a lowland tundra landscape in northern Siberia, Lena River delta, Biogeosciences, 12(4), 977–990, doi:10.5194/bg-12-977-2015, 2015.

Langer, M., Westermann, S., Boike, J., Kirillin, G., Grosse, G., Peng, S. and Krinner, G.: Rapid degradation of permafrost underneath waterbodies in tundra landscapes-Toward a representation of thermokarst in land surface models, J. Geophys. Res. Earth Surf., 121(12), 2446–2470, doi:10.1002/2016JF003956, 2016.

Liljedahl, A. K., Boike, J., Daanen, R. P., Fedorov, A. N., Frost, G. V., Grosse, G., Hinzman, L. D., Iijma, Y., Jorgenson, J. C., Matveyeva, N., Necsoiu, M., Raynolds, M. K., Romanovsky, V. E., Schulla, J., Tape, K. D., Walker, D. A., Wilson, C., Yabuki, H. and Zona, D.: Pan-Arctic ice-wedge degradation in warming permafrost and influence on tundra hydrology, Nat. Geosci., 9(April), 312–318, doi:10.1038/ngeo2674, 2016.

Lindgren, A., Hugelius, G. and Kuhry, P.: Extensive loss of past permafrost carbon but a net accumulation into present-day soils, Nature, 560(7717), 219–222, doi:10.1038/s41586-018-0371-0, 2018.

Liston, G. E. and Hiemstra, C. A.: The Changing Cryosphere: Pan-Arctic Snow Trends (1979–2009), J. Clim., 24(21), 5691–5712, doi:10.1175/JCLI-D-11-00081.1, 2011.

Luoto, M., Fronzek, S. and Zuidhoff, F. S.: Spatial modelling of palsa mires in relation to climate in northern Europe, Earth Surf. Process. Landforms, 29(11), 1373–1387, doi:10.1002/esp.1099, 2004.

Mamet, S. D., Chun, K. P., Kershaw, G. G. L., Loranty, M. M. and Peter Kershaw, G.: Recent Increases in Permafrost Thaw Rates and Areal Loss of Palsas in the Western Northwest Territories, Canada, Permafr. Periglac. Process., 28(4), 619–633, doi:10.1002/ppp.1951, 2017.

Martin, L. C. P. C. P., Nitzbon, J., Aas, K. S. S., Etzelmüller, B., Kristiansen, H. and Westermann, S.: Stability Conditions of Peat Plateaus and Palsas in Northern Norway, J. Geophys. Res. Earth Surf., 124(3), 1–15, doi:10.1029/2018JF004945, 2019.

McGuire, A. D., Lawrence, D. M., Koven, C., Clein, J. S., Burke, E., Chen, G., Jafarov, E., MacDougall, A. H., Marchenko, S., Nicolsky, D., Peng, S., Rinke, A., Ciais, P., Gouttevin, I., Hayes, D. J., Ji, D., Krinner, G., Moore, J. C., Romanovsky, V., Schädel, C., Schaefer, K., Schuur, E. A. G. and Zhuang, Q.: Dependence of the evolution of carbon dynamics in the northern permafrost region on the trajectory of climate change, Proc. Natl. Acad. Sci., 115(15), 3882–3887, doi:10.1073/pnas.1719903115, 2018.

Monin, A. S. and Obukhov, A. M.: Basic laws of turbulent mixing in the surface layer of the atmosphere, Contrib. Geophys. Inst. Acad. Sci. USSR, 151, 163–187, 1954.

Morgalev, Y. N., Lushchaeva, I. V., Morgaleva, T. G., Kolesnichenko, L. G., Loiko, S. V., Krickov, I. V., Lim, A., Raudina, T. V., Volkova, I. I., Shirokova, L. S., Morgalev, S. Y., Vorobyev, S. N., Kirpotin, S. N. and Pokrovsky, O. S.: Bacteria primarily metabolize at the active layer/permafrost border in the peat core from a permafrost region in western Siberia, Polar Biol., 40(8), 1645–1659, doi:10.1007/s00300-017-2088-1, 2017.

Motorin, A. S., Bukin, A. V and Iglovikov, A. V: Water-physical properties of drained peat soils of Northern Trans-Ural forest-steppe zone, IOP Conf. Ser. Earth Environ. Sci., 90, 012053, doi:10.1088/1755-1315/90/1/012053, 2017.

Natali, S. M., Watts, J. D., Rogers, B. M., Potter, S., Ludwig, S. M., Selbmann, A.-K., Sullivan, P. F., Abbott, B.

https://doi.org/10.5194/tc-2020-338
Preprint. Discussion started: 22 December 2020

W., Arndt, K. A., Birch, L., Björkman, M. P., Bloom, A. A., Celis, G., Christensen, T. R., Christiansen, C. T., Commane, R., Cooper, E. J., Crill, P., Czimczik, C., Davydov, S., Du, J., Egan, J. E., Elberling, B., Euskirchen, E. S., Friborg, T., Genet, H., Göckede, M., Goodrich, J. P., Grogan, P., Helbig, M., Jafarov, E. E., Jastrow, J. D., Kalhori, A. A. M., Kim, Y., Kimball, J. S., Kutzbach, L., Lara, M. J., Larsen, K. S., Lee, B.-Y., Liu, Z., Loranty, M. M., Lund, M., Lupascu, M., Madani, N., Malhotra, A., Matamala, R., McFarland, J., McGuire, A. D., Michelsen, A., Minions, C., Oechel, W. C., Olefeldt, D., Parmentier, F.-J. W., Pirk, N., Poulter, B., Quinton, W., Rezanezhad, F., Risk, D., Sachs, T., Schaefer, K., Schmidt, N. M., Schuur, E. A. G., Semenchuk, P. R., Shaver, G., Sonnentag, O., Starr, G., Treat, C. C., Waldrop, M. P., Wang, Y., Welker, J., Wille, C., Xu, X., Zhang, Z., Zhuang, Q. and Zona, D.: Large loss of CO2 in winter observed across the northern permafrost region, Nat. Clim. Chang., 9(11), 852–857, doi:10.1038/s41558-019-0592-8, 2019.

Nitzbon, J., Langer, M., Westermann, S., Martin, L., Aas, K. S. and Boike, J.: Pathways of ice-wedge degradation in polygonal tundra under different hydrological conditions, Cryosph., 13(4), 1089–1123, doi:10.5194/tc-13-1089-2019, 2019.

Nitzbon, J., Westermann, S., Langer, M., Martin, L. C. P., Strauss, J., Laboor, S. and Boike, J.: Fast response of cold ice-rich permafrost in northeast Siberia to a warming climate, Nat. Commun., 11(1), 2201, doi:10.1038/s41467-020-15725-8, 2020.

Nwaishi, F. C., Morison, M. Q., Van Huizen, B., Khomik, M., Petrone, R. M. and Macrae, M. L.: Growing season CO 2 exchange and evapotranspiration dynamics among thawing and intact permafrost landforms in the Western Hudson Bay lowlands, Permafr. Periglac. Process., ppp.2067, doi:10.1002/ppp.2067, 2020.

O'Gorman, P. a.: Contrasting responses of mean and extreme snowfall to climate change, Nature, 512(7515), 416–418, doi:10.1038/nature13625, 2014.

Obu, J., Westermann, S., Bartsch, A., Berdnikov, N., Christiansen, H. H., Dashtseren, A., Delaloye, R., Elberling, B., Etzelmüller, B., Kholodov, A., Khomutov, A., Kääb, A., Leibman, M. O., Lewkowicz, A. G., Panda, S. K., Romanovsky, V., Way, R. G., Westergaard-Nielsen, A., Wu, T., Yamkhin, J. and Zou, D.: Northern Hemisphere permafrost map based on TTOP modelling for 2000–2016 at 1 km2 scale, Earth-Science Rev., 193(October 2018), 299–316, doi:10.1016/j.earscirev.2019.04.023, 2019.

Parviainen, M. and Luoto, M.: Climate envelopes of mire complex types in Fennoscandia, Geogr. Ann. Ser. A Phys. Geogr., 89(2), 137–151, doi:10.1111/j.1468-0459.2007.00314.x, 2007.

Payette, S., Delwaide, A., Caccianiga, M. and Beauchemin, M.: Accelerated thawing of subarctic peatland permafrost over the last 50 years, Geophys. Res. Lett., 31(18), 1–4, doi:10.1029/2004GL020358, 2004.

Raynolds, M. K., Jorgenson, J. C., Jorgenson, M. T., Kanevskiy, M., Liljedahl, A. K., Nolan, M., Sturm, M. and Walker, D. A.: Landscape impacts of 3D-seismic surveys in the Arctic National Wildlife Refuge, Alaska, Ecol. Appl., 30(7), 1–20, doi:10.1002/eap.2143, 2020.

Sannel, A. B. K.: Ground temperature and snow depth variability within a subarctic peat plateau landscape, Permafr. Periglac. Process., 31(2), 255–263, doi:10.1002/ppp.2045, 2020.

Sannel, A. B. K. and Kuhry, P.: Warming-induced destabilization of peat plateau/thermokarst lake complexes, J. Geophys. Res. Biogeosciences, 116(3), doi:10.1029/2010JG001635, 2011.

Sannel, A. B. K., Hugelius, G., Jansson, P. and Kuhry, P.: Permafrost Warming in a Subarctic Peatland - Which Meteorological Controls are Most Important?, Permafr. Periglac. Process., 27(2), 177–188, doi:10.1002/ppp.1862, 2016.

Schuur, E. A. G., Vogel, J. G., Crummer, K. G., Lee, H., Sickman, J. O. and Osterkamp, T. E.: The effect of permafrost thaw on old carbon release and net carbon exchange from tundra, Nature, 459(7246), 556–559, doi:10.1038/nature08031, 2009.

Schuur, E. A. G., McGuire, A. D., Grosse, G., Harden, J. W., Hayes, D. J., Hugelius, G., Koven, C. D. and Kuhry, P.: Climate change and the permafrost carbon feedback, Nature, 520(January 2016), 171–179, doi:10.1038/nature14338, 2015.

Seppälä, M.: The term "palsa," Zeitschrift für Geomorphol., 16(4), 463, 1972.

Seppälä, M.: Palsas and related forms, Adv. Periglac. Geomorphol., 247–278, 1988.

Seppälä, M.: Synthesis of studies of palsa formation underlining the importance of local environmental and physical characteristics, Quat. Res., 75(2), 366–370, doi:10.1016/j.yqres.2010.09.007, 2011.

Serikova, S., Pokrovsky, O. S., Ala-Aho, P., Kazantsev, V., Kirpotin, S. N., Kopysov, S. G., Krickov, I. V., Laudon, H., Manasypov, R. M., Shirokova, L. S., Soulsby, C., Tetzlaff, D. and Karlsson, J.: High riverine CO2

https://doi.org/10.5194/tc-2020-338
Preprint. Discussion started: 22 December 2020

emissions at the permafrost boundary of Western Siberia, Nat. Geosci., 11(11), 825–829, doi:10.1038/s41561-018-0218-1, 2018.

Sherstyukov, A. B. and Sherstyukov, B. G.: Spatial features and new trends in thermal conditions of soil and depth of its seasonal thawing in the permafrost zone, Russ. Meteorol. Hydrol., 40(2), 73–78, doi:10.3103/S1068373915020016, 2015.

Sjöberg, Y., Coon, E., K. Sannel, A. B., Pannetier, R., Harp, D., Frampton, A., Painter, S. L. and Lyon, S. W.: Thermal effects of groundwater flow through subarctic fens: A case study based on field observations and numerical modeling, Water Resour. Res., 52(3), 1591–1606, doi:10.1002/2015WR017571, 2016.

Skamarock, W. C. and Klemp, J. B.: A time-split nonhydrostatic atmospheric model for weather research and forecasting applications, J. Comput. Phys., 227(7), 3465–3485, doi:10.1016/j.jcp.2007.01.037, 2008.

Sollid, J. and Sørbel, L.: Palsa Bogs as a Climate Indicator-Examples, , 27(4), 287–291 [online] Available from: http://www.jstor.org/stable/4314737, 1998.

Teufel, B. and Sushama, L.: Abrupt changes across the Arctic permafrost region endanger northern development, Nat. Clim. Chang., 9(11), 858–862, doi:10.1038/s41558-019-0614-6, 2019.

Thibault, S. and Payette, S.: Recent permafrost degradation in bogs of the James Bay area, northern Quebec, Canada, Permafr. Periglac. Process., 20(4), 383–389, doi:10.1002/ppp.660, 2009.

Turetsky, M. R., Abbott, B. W., Jones, M. C., Anthony, K. W., Olefeldt, D., Schuur, E. A. G., Grosse, G., Kuhry, P., Hugelius, G., Koven, C., Lawrence, D. M., Gibson, C., Sannel, A. B. K. and McGuire, A. D.: Carbon release through abrupt permafrost thaw, Nat. Geosci., 13(2), 138–143, doi:10.1038/s41561-019-0526-0, 2020.

Vionnet, V., Brun, E., Morin, S., Boone, A., Faroux, S., Le Moigne, P., Martin, E. and Willemet, J.-M.: The detailed snowpack scheme Crocus and its implementation in SURFEX v7.2, Geosci. Model Dev., 5(3), 773–791, doi:10.5194/gmd-5-773-2012, 2012.

Walczak, R. and Rovdan, E.: Water retention characteristics of peat and sand mixtures, Int. Agrophysics, (12), 161–165, 2002.

Way, R. G., Lewkowicz, A. G. and Zhang, Y.: Characteristics and fate of isolated permafrost patches in coastal Labrador, Canada, Cryosph., 12(8), 2667–2688, doi:10.5194/tc-12-2667-2018, 2018.

Westermann, S., Langer, M., Boike, J., Heikenfeld, M., Peter, M., Etzelmüller, B. and Krinner, G.: Simulating the thermal regime and thaw processes of ice-rich permafrost ground with the land-surface model CryoGrid 3, Geosci. Model Dev., 9(2), 523–546, doi:10.5194/gmd-9-523-2016, 2016.